Structural Basis for Rational Design of Inhibitors Targeting *Trypanosoma cruzi* Sterol 14α-Demethylase: Two Regions of the Enzyme Molecule Potentiate Its Inhibition

Laura Friggeri,[†,#] Tatiana Y. Hargrove,[†] Girish Rachakonda,[‡] Amanda D. Williams,[‡] Zdzislaw Wawrzak,[§] Roberto Di Santo,[∥] Daniela De Vita,[∥] Michael R. Waterman,[†] Silvano Tortorella,[∥] Fernando Villalta,[‡] and Galina I. Lepesheva*,[†,⊥]

[†]Department of Biochemistry, School of Medicine, Vanderbilt University, Nashville, Tennessee 37232, United States

[‡]Department of Microbiology and Immunology, Meharry Medical College, Nashville, Tennessee 37208, United States

[§]Synchrotron Research Center, Life Science Collaborative Access Team, Northwestern University, Argonne, Illinois 60439, United States

[∥]"Istituto Pasteur-Fondazione Cenci Bolognetti", Department of "Chimica e Tecnologie del Farmaco", Sapienza University of Rome, Rome, 00185, Italy

[⊥]Center for Structural Biology, Vanderbilt University, Nashville, Tennessee 37232, United States

S *Supporting Information*

T. cruzi EC$_{50}$=1.2 nM

T. cruzi EC$_{50}$=1.0 nM
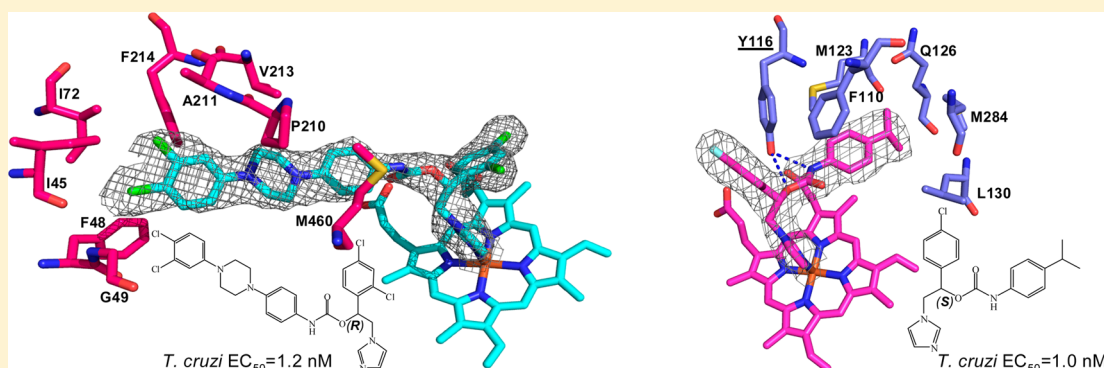
ABSTRACT: Chagas disease, which was once thought to be confined to endemic regions of Latin America, has now gone global, becoming a new worldwide challenge with no cure available. The disease is caused by the protozoan parasite *Trypanosoma cruzi*, which depends on the production of endogenous sterols, and therefore can be blocked by sterol 14α-demethylase (CYP51) inhibitors. Here we explore the spectral binding parameters, inhibitory effects on *T. cruzi* CYP51 activity, and antiparasitic potencies of a new set of β-phenyl imidazoles. Comparative structural characterization of the *T. cruzi* CYP51 complexes with the three most potent inhibitors reveals two opposite binding modes of the compounds ((*R*)-6, EC$_{50}$ = 1.2 nM, vs (*S*)-2/(*S*)-3, EC$_{50}$ = 1.0/5.5 nM) and suggests the entrance into the CYP51 substrate access channel and the heme propionate-supporting ceiling of the binding cavity as two distinct areas of the protein that enhance molecular recognition and therefore could be used for the development of more effective antiparasitic drugs.

■ INTRODUCTION

American trypanosomiasis (Chagas disease) is a vector-borne anthropozoonosis, the life-long infection caused by the protozoan pathogen *Trypanosoma cruzi*.[1] For centuries the disease has been a major cause of mortality and morbidity in South and Central America, where it still remains endemic in 21 countries, resulting in about 14,000 deaths per year,[2] mainly due to heart failure, that is the most typical pathology of the chronic form of this infection. During the last years, Chagas disease has begun receiving attention as an emerging global medical problem,[3,4] predominantly because of human and insect vector (kissing bug) migration, but also as a result of the lack of awareness and diagnostics in nonendemic areas, often leading to transfusion of infected blood; transplantation of infected organs, food, and drink contaminations; as well as HIV coinfections and congenital transmission.[5,6] Thus, recent estimates indicate that there could be up to 1 million cases of Chagas disease in the USA, a significant portion of which, particularly in the southern states, are of autochthonous vector-borne origin.[7,8]
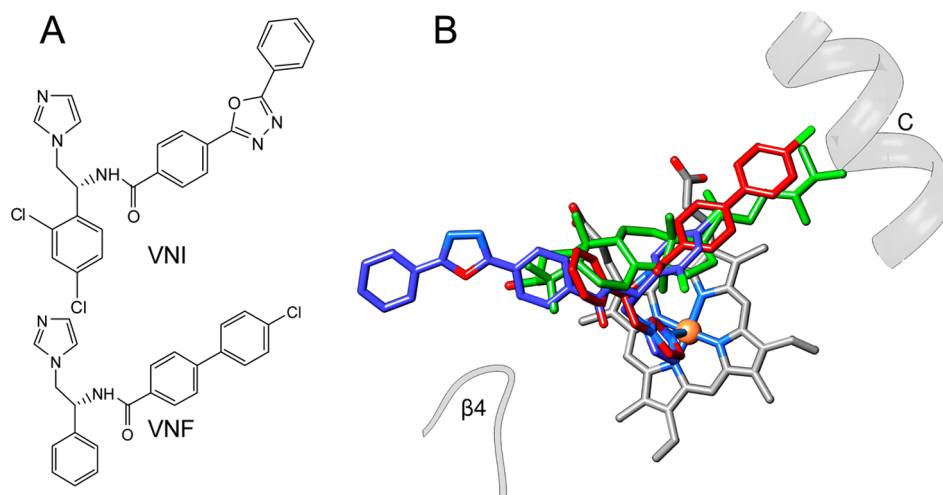
Figure 1. VNI and VNF. (A) Structural formulas. (B) Orientation in the CYP51 active site. Distal P450 view. VNI, VNF, and the *T. cruzi* CYP51 substrate eburicol are shown in blue, red, and green, respectively. The carbon atoms of the heme are colored in gray. Helix C and the β4-hairpin are outlined as semitransparent gray ribbons.

Despite the severity of the problem and ~25 million people at risk of infection, nifurtimox and benznidazole are the only drugs available for treatment of Chagas disease. Although generally rather helpful in the acute stage, they vary significantly in their efficiency against different *T. cruzi* strains,[9] they have considerable adverse side effects, and their success in curing chronic Chagas disease is still debated.[10,11] Despite these limitations, pharmaceutical companies remain reluctant to invest resources in the development of new antichagasic chemotherapies, because of the lack of assurances that they can make a return on their investment, since historically Chagas disease has been known to mostly affect the poorest. As a result, the majority of efforts to fill the gap for new antichagasic drugs have come from academia. Repurposing of antifungal azoles, the drugs that act via sterol biosynthesis by inhibiting the cytochrome P450 enzyme sterol 14α-demethylase (CYP51)[12] so far have been particularly successful (reviewed in refs 1 and 13). The FDA-approved drug posaconazole and an investigational prodrug of ravuconazole (Eisai) are presently in phase 2 clinical trials for Chagas.[3] Some other azole derivatives, e.g. the anticancer drug candidate tipifarnib[14,15] or (S)-2-(5-((1-(biphenyl-4-ylmethyl)-1H-imidazol-5-yl)methylamino)-biphenyl-2-ylcarboxamido)-4-(methylthio)butanoic acid (FTI-2220),[16] were also shown to display potent antiparasitic effects and are under development. Later, several new experimental heterocyclic compounds, both azoles[17,18] and pyridines[19,20] were identified as potent and selective inhibitors of *T. cruzi* CYP51 (the protein has less than 25% amino acid sequence identity to its fungal orthologs[21]) and structurally characterized in complex with the target enzyme.[18,20,22,23] Most recently, one of these inhibitors, VNI, has been shown to cure both the acute and chronic forms of Chagas disease in mice.[24]

Being the most potent *T. cruzi* CYP51 inhibitors that we have discovered,[17] VNI and VNF share high structural similarity. The phenethylimidazole portion of these molecules is connected via the polar linker (carboxamide fragment) to the lipophilic arm that consists of either a 2-ring (VNF) or a 3-ring (VNI) linear polycycle (Figure 1A). In the CYP51 costructures, VNI and VNF are coordinated to the P450 heme iron through their imidazole ring nitrogen (N3). The other two portions of the inhibitor molecules, however, adopt an opposite orientation:[23] while the 3-ring arm of VNI lies in the CYP51

substrate access channel, the 2-ring arm of VNF is positioned within the deepest segment of the CYP51 binding cavity, the hydrophobic area that accommodates the aliphatic tail of the sterol substrate (Figure 1B).

In this work we prepared a set of 12 β-phenyl imidazoles and analyzed their structure−activity relationship in terms of *T. cruzi* CYP51 binding parameters, inhibition of reconstituted enzymatic reaction *in vitro*, and antiparasitic effects against GFP-expressing *T. cruzi* amastigotes. Three most efficient compounds were cocrystallized with *T. cruzi* CYP51, the X-ray costructures uncovering two basic approaches that can be utilized to further enhance potencies of CYP51 inhibitors.

■ RESULTS AND DISCUSSION

Medicinal Chemistry. Compound **1** (MW 368, clogP 5.3, tPSA 41.9 (ChemDraw)) has been previously characterized as a potential antifungal agent and revealed quite promising results.[25] Its structural resemblance to VNF has prompted us to expand our work on this inhibitory chemotype by modifying the chemical structure of **1** as shown in Table 1 followed by testing the original molecule and its derivatives against *T. cruzi* and its potential target enzyme *T. cruzi* sterol 14α-demethylase. In all cases the polar linker between the phenethylimidazole moiety and the opposite arm of the new structures was replaced with the carbamate group, because it was previously found to have higher hydrolytic stability in liver microsomes than the ester group of **1**.[26] Our major focus on modification of the side chain arm of the compounds was based on the observation that variations in the composition of this portion of a β-phenyl imidazole molecule (a) could be crucial for its potency to inhibit CYP51 activity[17] and (b) may alter its orientation within the enzyme active site.[23] In compounds **2** (MW 384, clogP 4.9, tPSA 53.9) and **3** (MW 367, clogP 4.3, tPSA 53.9), the side chain arm is one aromatic ring shorter than it is in **1**, and in the para-position of the β-phenyl ring they have either Cl atom (**2**) or smaller and more polar F atom (**3**). Compound **4** (MW 357, clogP 1.8, tPSA 69.5), similarly to **3**, also has fluorine in the para-position of the β-phenyl ring; however, its side chain arm, instead of the bulky aromatic ring, carries a flexible three-carbon atom aliphatic chain ending with the polar imidazole ring. The arm of compound **5** (MW 494, clogP 5.6, tPSA
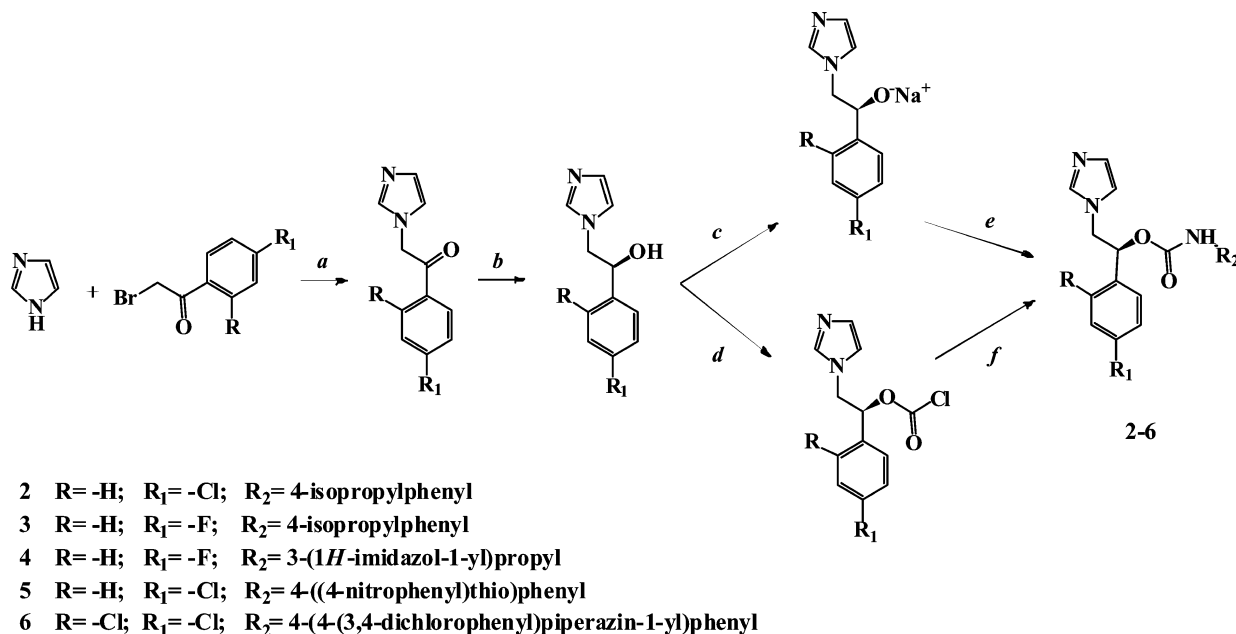
Table 1. Structural Formulas, *T. cruzi* CYP51 Spectral Binding Parameters, Inhibition of Enzymatic Activity, and Antiparasitic Effects of Compounds 1−6[a]

| Compound	Structure	CYP51 spectral response			CYP51 substrate conversion at I/E=2 (%)[b]	*T. cruzi* amastigotes[c]	
		ΔA_{max}/cm/ nmol P450 (optical units)	K_s (μM)	Binding efficiency ($\Delta A_{max}/K_s$)		EC_{50} (nM)	Inhibition at 10 nM (%)
1 (*R*)-		0.042±0.001	0.087±0.02	0.5	79.5±1.5	15±0.3	29.5±2.1
(*S*)-		0.043±0.001	0.046±0.01	0.9	0.7±0.2	1.2±0.1	76.3±7.1
2 (*R*)-		0.039±0.001	0.056±0.01	0.7	90.0±5.0	22±1.7	30.5±3.5
(*S*)- **(LFT)**[d]		0.044±0.001	0.032±0.01	1.4	1.9±0.2	1.0±0.1	74.5±13.4
3 (*R*)-		0.058±0.002	0.083±0.02	0.6	86.5±6.5	20±2.5	32.1±2.8
(*S*)- **(LFS)**[d]		0.047±0.001	0.032±0.01	1.4	8.5±3.5	5.5±0.7	69.3±4.2
4 (*R*)-		0.030±0.001	0.087±0.02	0.3	89.2±4.8	Nd	Nd
(*S*)-		0.030±0.0002	0.600±0.02	0.1	93.9±3.8	Nd	Nd
5 (*R*)-		0.063±0.09	0.715±0.29	0.1	52.5±2.5	2.5±0.1	62.5±3.5
(*S*)-		0.046±0.004	0.162±0.08	0.3	12.5±1.5	1.5±0.1	70.0±14.1
6 (*R*)- **(LFD)**[d]		0.042±0.001	0.064±0.03	0.7	0.8±0.1	1.2±0.1	83.0±9.9
(*S*)-		0.047±0.006	0.123±0.11	0.4	3.8±0.4	1.3±0.1	73.5±7.8

[a]The values represent mean ± standard deviation from three independent experiments. [b]1 h reaction (examples of HPLC profiles for compounds **2** and **6** are shown in Figure 3). [c]The corresponding values for posaconazole are EC_{50} = 5.0 nM ; inhibition at 10 nM = 64%. [d]Compounds cocrystallized with *T. cruzi* CYP51.

105.5) bears two aromatic rings linked via the sulfur atom, with the distal ring ending with a nitro group in the para-position. Compound **6** (MW 605, clogP 7.2, tPSA 60.4) is the largest of the molecules. It has two chlorine substituents in the ortho- and para-positions of the β-phenyl ring, while its long arm is composed of three rings linked in a linear sequence, with the distal aromatic ring being complemented with two chlorine atoms, in the 3- and 4- positions so that the total length of the arm (~18 Å) is close to the length of the CYP51 substrate access channel.[22]

In this study the compounds were prepared as (*R*)- and (*S*)-stereoisomers using enantioselective synthesis.[26] Briefly, the 2-(1*H*-imidazol-1-yl)-1-phenylethanones were obtained by condensation of 1*H*-imidazole and commercial bromoacetophenones[25] substituted in the ortho/para position with different halogens (Scheme 1a). In order to obtain the (*S*)-2-(1*H*-imidazol-1-yl)-1-phenylethanols, the keto group of 2-(1*H*-imidazol-1-yl)-1-phenylethanones was reduced to hydroxyl using as the catalyst RuCl(*p*-cymene)[(R,R)-Ts-DPEN] (Scheme 1b). Accordingly, RuCl(*p*-cymene)[(S,S)-Ts-DPEN] has been used as the catalyst to prepare the (*R*)-2-(1*H*-

Scheme 1. Enantioselective Synthesis of (S)-Stereoisomers of Compounds 2−6[a]

2   R= -H;   R$_1$= -Cl;   R$_2$= 4-isopropylphenyl
3   R= -H;   R$_1$= -F;   R$_2$= 4-isopropylphenyl
4   R= -H;   R$_1$= -F;   R$_2$= 3-(1*H*-imidazol-1-yl)propyl
5   R= -H;   R$_1$= -Cl;   R$_2$= 4-((4-nitrophenyl)thio)phenyl
6   R= -Cl;   R$_1$= -Cl;   R$_2$= 4-(4-(3,4-dichlorophenyl)piperazin-1-yl)phenyl

[a]Reagents and conditions. (*a*) DMF, 0 °C, 2 h; (*b*) CH$_2$Cl$_2$, RuCl(*p*-cymene)[(*R,R*)-Ts-DPEN], HCOOH, TEA, N$_{2(g)}$, 40 °C, 26 h; (*c*) anhydrous CH$_3$CN, NaH, 2 h, room temperature; (*d*) anhydrous CH$_3$CN, triphosgene, room temperature; overnight; (*e*) 4-isopropylphenyl isocyanate, room temperature, 48 h; (*f*) TEA, R$_2$-NH$_2$, room temperature, overnight.

Scheme 2. Synthesis of the Long Arm of Compound 6[a]
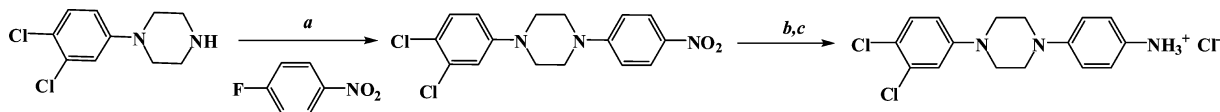
[a]Reagents and conditions. (*a*) CH$_3$CN, reflux, 2 h; (*b*) MeOH, H$_2$, Pd/C, 50 psi, room temperature, 4 h; (*c*) MeOH, HCl$_{(g)}$.

imidazol-1-yl)-1-phenylethanols. The −OH group was subsequently deprotonated with sodium hydride (*c*) or activated with triphosgene (*d*) in anhydrous CH$_3$CN in order to obtain sodium alkoxide and chloroformate. Then commercial 4-isopropylphenyl isocyanate, 2-(1*H*-imidazol-1-yl)propan-1-amine and 4-((4-nitrophenyl)thio)aniline have been added for preparing the side chain arms of compounds **2/3**, **4**, and **5**, respectively. (Scheme 1 *e,f*).

The long arm of compound **6** has been synthesized as shown in Scheme 2. The synthesis was performed by condensation of 1-fluoro-4-nitrobenzene with 1-(3,4-dichlorophenyl)piperazine (*a*). Then the nitro group of 1-(3,4-dichlorophenyl)-4-(4-nitrophenyl)piperazine was converted to an amino group by reduction with H$_2$ using Pd/C as the catalyst (*b*) to produce 4-[4-(3,4-dichlorophenyl)piperazin-1-yl]aniline; and the final amine was stabilized as 4-[4-(3,4-dichlorophenyl)piperazin-1-yl] anilinium chloride by HCl$_{(g)}$ flow in the same reaction environment (*c*).

T. cruzi CYP51 Spectral Responses vs Inhibition of Reconstituted Sterol 14α-Demethylase Activity in Vitro. In the resting ferric form the heme iron of CYP51 enzymes is present in the low spin state, with a water molecule serving as its sixth axial (distal) ligand. This results in the P450 absorbance spectrum with the Soret band maximum at around 417 nm. Binding of azoles or other heterocyclic compounds replaces the water molecule in the heme iron coordination sphere with the basic nitrogen atom, causing a so-called red shift in the Soret band maximum. Accordingly, in the difference spectra a trough and a peak appear on the left and the right sides of an isosbestic point. These spectral changes, also known as a type 2 spectral response, are widely used to identify new P450 binding ligands. However, even very low spectral dissociation constants do not necessarily reflect the compound's potency to inhibit CYP51 activity, because during the reaction many ligands can still be replaced in the enzyme active center by the substrate.[17,20,22]

Twelve imidazole derivatives tested in this study act in good agreement with this observation. As expected, all of them cause typical type 2 spectral responses in the CYP51 heme iron, with the apparent spectral dissociation constants (K_s) being mostly in the nanomolar range, and therefore should be defined as tight binding ligands (Table 1, Figure 2).

However, particularly in the case of compounds **1−3**, the inhibitory effects of the (*R*)- and (*S*)-enantiomers on the CYP51 activity appeared to be quite "independent" of the binding parameters. Thus, (*S*)-**2** displayed only 2-fold higher apparent binding efficiency than (*R*)-**2**, yet its inhibitory effect on the substrate conversion is ∼50-fold stronger (Table 1, Figure 3A). The same tendency was observed for **1** and **3**. In all these three cases, the (*S*)-enantiomers are much more potent as *T. cruzi* CYP51 inhibitors than the (*R*)-enantiomers. The (*R*)- and (*S*)- enantiomers of compounds **4−6**, on the opposite, do not differ that drastically in their potencies to inhibit *T. cruzi* CYP51 reaction (Table 1, Figure 3B), although significant variations can be seen in the apparent K_s's, particularly for **4** ((*S*)- ≫ (*R*)-). Only the enantiomers of compound **6** presented
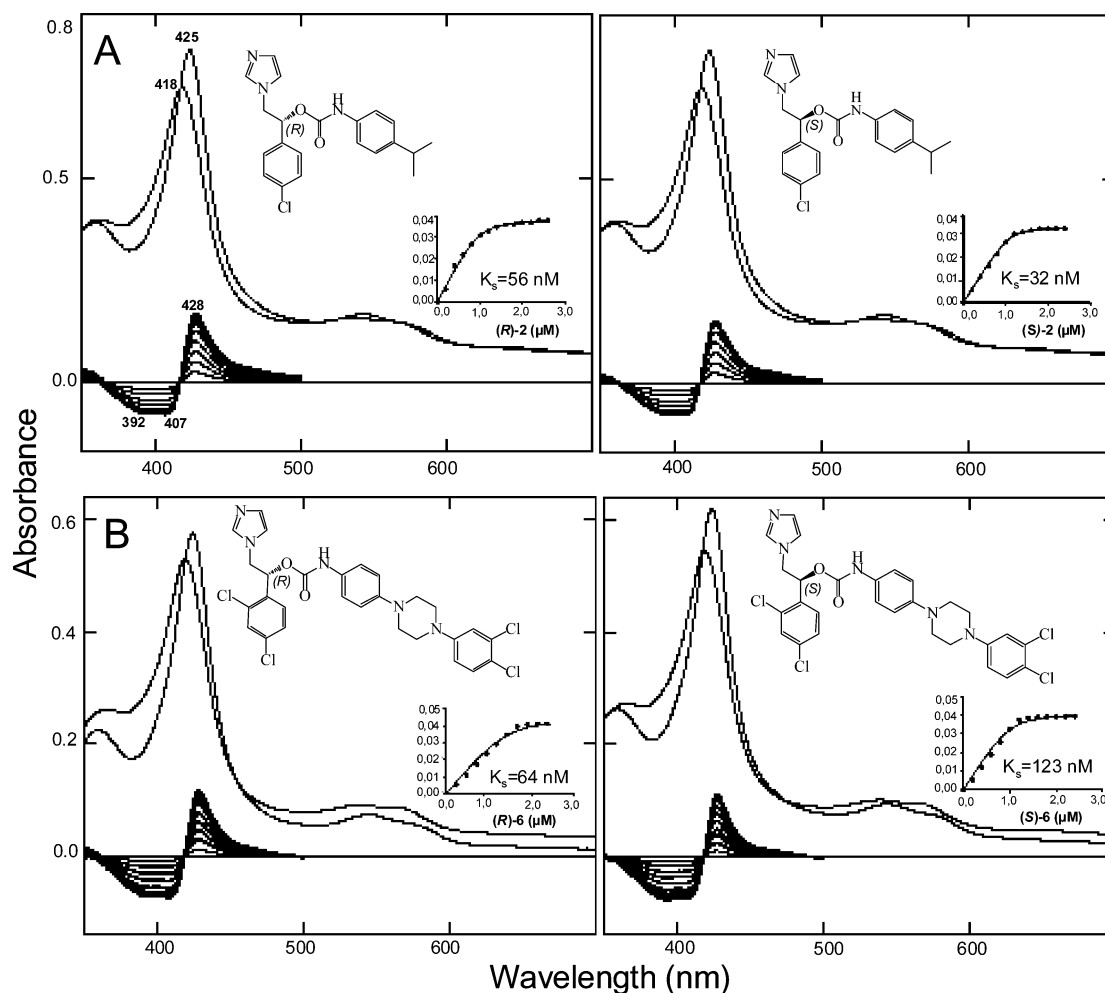
Figure 2. Spectral responses of *T. cruzi* CYP51 to the binding of (A) (*R*)- and (*S*)- enantiomers of compound **2**; [P450] = 1.1 μM and (B) (*R*)- and (*S*)- enantiomers of compound **6**; [P450] = 0.9 μM. Optical path length 5 cm. Upper: absolute absorbance spectra, the Soret band maximum shifts to the right (from 418 to 425 nm). Lower: difference spectra upon titration with the ligands (titration step 0.2 μM). Insets: titration curves showing absorbance changes per 1 cm optical path/1 nmol P450 upon increasing ligand concentrations (processed with the Morrison equation).

rather good correlation between the CYP51 inhibition and binding parameters. Nevertheless, their spectral dissociation constants are either higher ((*S*)-, K_s = 0.123 μM) or within ((*R*)-, K_s = 0.064 μM) the range of the values calculated for the (*R*)- enantiomers of compounds **1**−**3** (weak *T. cruzi* CYP51 inhibitors).

Another unusual observation, which we encountered upon titration of *T. cruzi* CYP51 with compound **6** (both (*R*)- and (*S*)-enantiomers), was the very slow increase in the amplitude of the type 2 spectral response over time. This increase was most pronounced when the enzyme concentration considerably exceeded the concentration of the ligand. To our knowledge, such an increase has not been previously reported for any other CYPs. Since none of the other compounds tested in this work produced such an effect, we conducted the same experiments with other known *T. cruzi* CYP51 inhibitors, and we found that a somewhat similar pattern is also produced by ketoconazole, another CYP51 inhibitor with a rigid long arm but not by VNI (Figure 4). The current lack of any information on the topic might be related to the fact that traditionally the measurements of P450 spectral responses have been mostly conducted at higher ligand/P450 molar ratios.

Crystallographic Analysis. In order to expand our understanding of the molecular basis that underlies the

potencies of CYP51 inhibitors as well as to shed light on the features that may have caused the observed peculiarities in their binding behavior, we crystallized *T. cruzi* CYP51 in the presence of (*S*)-**2**, (*S*)-**3**, and (*R*)-**6**, which are among the strongest inhibitors of the enzyme identified in this study (Table 1), and we determined the X-ray structures of their complexes. Table 2 summarizes the diffraction and refinement statistics. As expected, (*R*)-**6** (ligand PDB ID LFD, molecular volume 1,040 Å^3, surface area 880 Å^2) adopts a VNI-like orientation, with its longer arm protruding ∼7 Å further toward the entrance into the substrate access channel (Figure 5A), while the vectors of (*S*)-**2** (ligand PDB ID LFT, molecular volume 870 Å^3, surface area 725 Å^2) and (*S*)-**3** (ligand PDB ID LFS, molecular volume 849 Å^3, surface area 709 Å^2) follow that of VNF, being directed toward helix C (Figure 5B). The amino acid residues that contact each inhibitor are listed in Table 3, and their location in the *T. cruzi* CYP51 structure is seen in Figure 5.

Overall, the structures suggest that the potency of LFD (20 inhibitor contacting residues) must be enhanced by the formation of the surface binding subsite (Figure 6A−C, Supporting Information Figure S1), the rearrangement that was first observed in the structure of posaconazole-bound *T. cruzi* CYP51 [3K1O].[23] When two molecules of CYP51-LFD
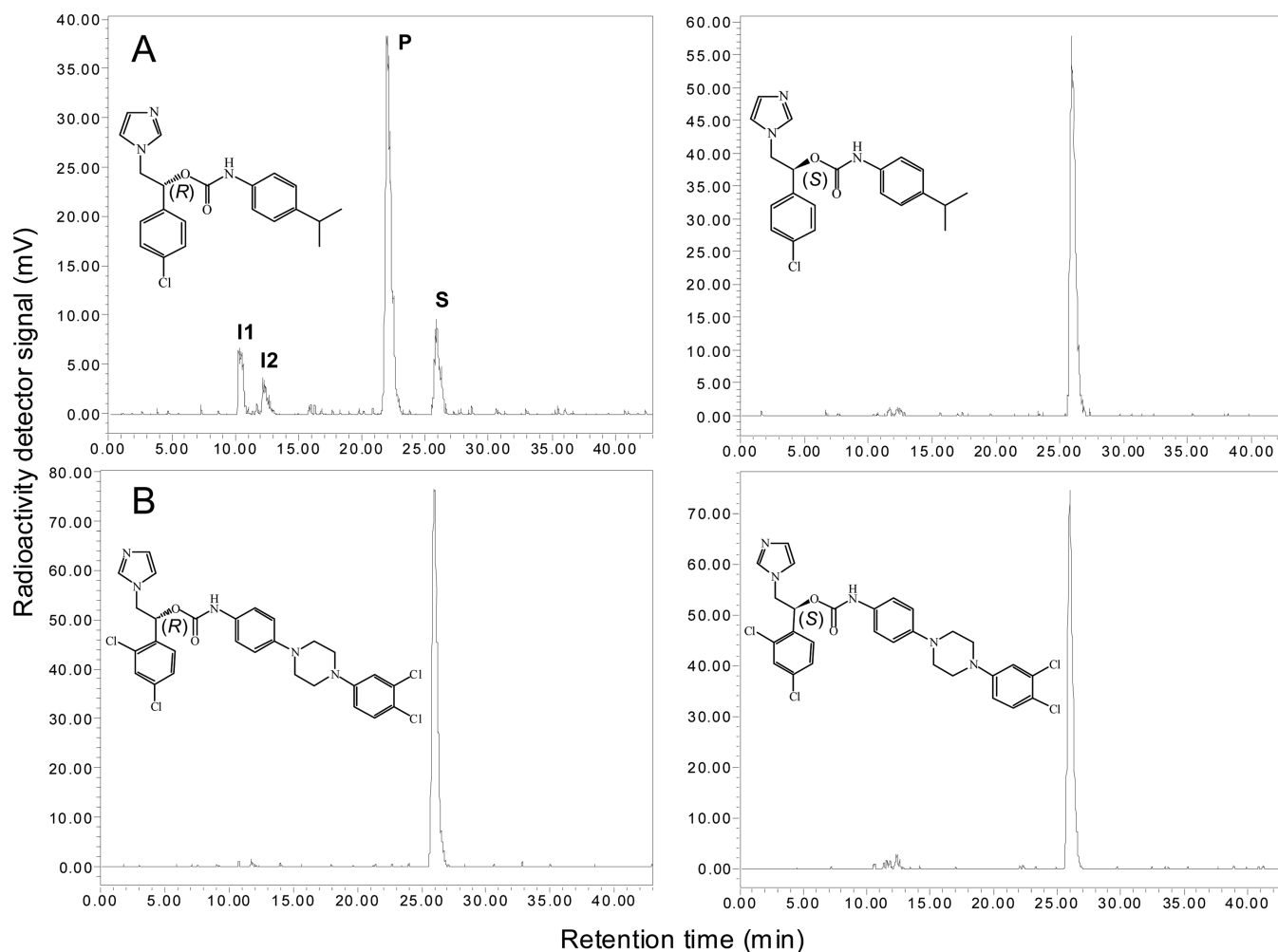
Figure 3. HPLC profiles of eburicol conversion by *T. cruzi* CYP51 in the presence of a 2-fold molar excess of the inhibitor over the enzyme. 1 h reaction. (A) (*R*)- and (*S*)-Enantiomers of compound **2**; (B) (*R*)- and (*S*)-Enantiomers of compound **6**. S, substrate (4,4,14-trimethylergosta-8-en-3ß-ol); I1, 14α-carboxyalcohol intermediate; I2, 14α-carboxyaldehyde intermediate; P, 14α-demethylated product (4,4-dimethylergosta-8,14-dien-3ß-ol).

(this structure has two molecules in the asymmetric unit (Table 2)) are superimposed with CYP51-LFT and CYP51-LFS, it is clearly seen that in the complex with LFD the secondary structural elements that form the entrance into the CYP51 substrate access channel are getting better organized, particularly helix F″, whose density in the complexes of *T. cruzi* CYP51 with smaller molecules is either missing (VNF [3KSW],[23] fluconazole [3KHM],[23] NEU [4H6O][18]) or appears to be more looplike (LFT and LFS (Figure 6C)). Moreover, some residues, e.g. F214, P210 (F″), I45 (A′), I72 (β1-1), move 1−1.5 Å closer toward the LFD 1,2-dichlorobenzene ring (Figure 6B), which, as a result, forms van der Waals contacts with 8 amino acids around the channel entrance (a possible example of a "localized" induced fit in CYP51). These multiple contacts between the enzyme and inhibitor are clearly decreasing the entrance flexibility (Supporting Information Figure S2A) and may prevent the CYP51 channel from opening, making it harder for the substrate molecule to replace the inhibitor, e.g. upon P450 reduction. On the other hand, LFD does not induce any significant rearrangements around the CYP51 heme binding area, which might explain why the (*R*)- and (*S*)-enantiomers of this compound would have similar inhibitory potencies and display similar apparent binding efficiencies. The observed

time-dependent increase in the spectral response of the P450 heme iron to the binding of the LFD nitrogen might be connected with some repositioning of the proximal to the heme portion of the inhibitor molecule, as even in the crystal lattice the two medium rings of this compound display obvious differences in their conformations (Figure 6B,E).

Although only 16 of the *T. cruzi* CYP51 amino acid residues lie at the distance <4.5 Å from LFT and LFS (Figure 5B, Table 3), which are much smaller molecules than LFD, their complexes with the enzyme are strengthened by the H-bonds with Y116. In both these structures the side chain hydroxyl of Y116 looses its contact with the heme ring D propionate,[27] shifts 1.5 Å toward the inhibitor, and interacts with the O and N atoms of its carbamic fragment (Figure 6 E,F). This change in the Y116 position increases the flexibility of the heme (Supporting Information Figure S2B) and allows the *p*-cymene moiety of the inhibitors to protrude deeper into the CYP51 binding cavity. Enhancement of the LFT/LFS complexes with CYP51 by the H-bond formation elucidates the importance of (*S*)-stereochemistry for the inhibitory potency of compounds **2** (LFT) and **3** (LFS), because the opposite orientation of the carbamic fragment in the (*R*)-enantiomers is not favorable for hydrogen bonding. It also provides a possible explanation for the observed "discrepancies" between the spectral binding
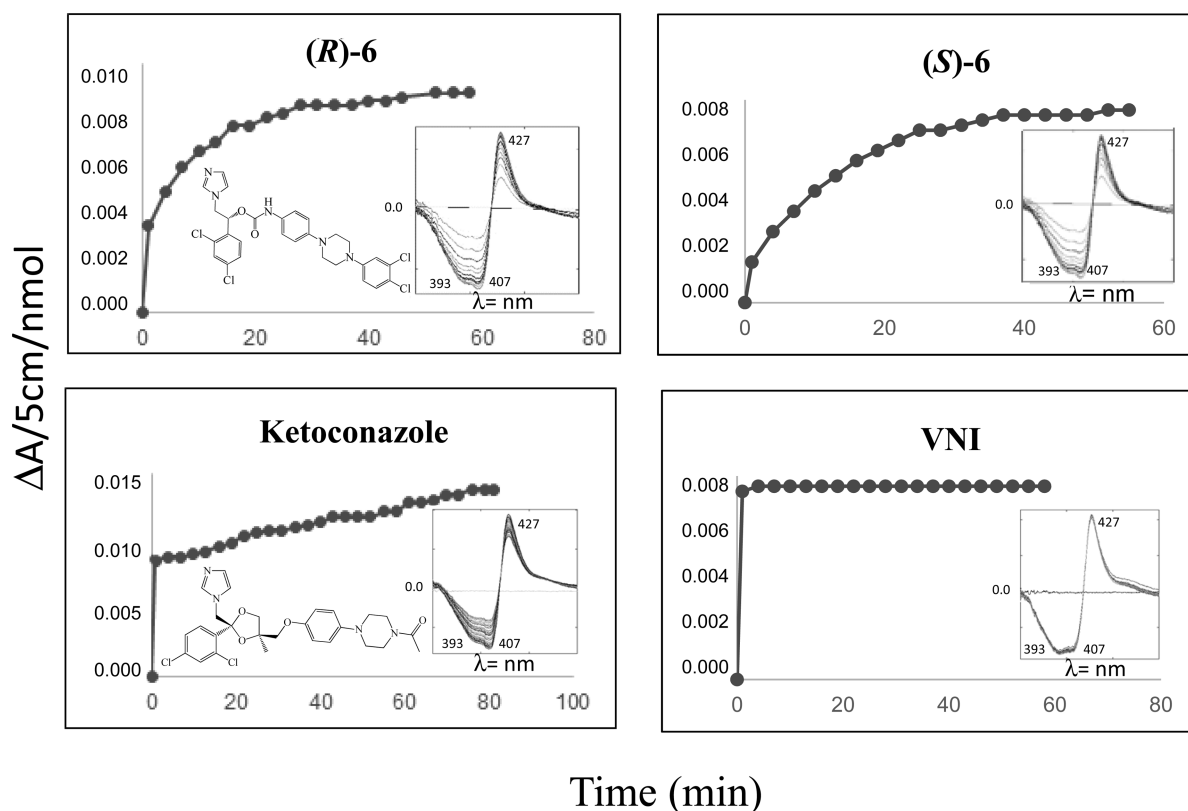
Figure 4. Time course of spectral responses of *T. cruzi* CYP51 (1.0 μM) to the addition of 0.2 μM of the heme-coordinating ligands.

parameters and inhibition (Table 1), since the H-bond formation might not influence the spectral response of the P450 heme iron to the imidazole nitrogen coordination, which apparently occurs fast and easily for both (*R*)- and (*S*)-enantiomers. Finally, combination of biochemical and structural data implies that compounds **4** and **5** are most likely to bind to *T. cruzi* CYP51 in the LFD orientation: (1) the arm of **5** (~15 Å) is probably too long and the imidazole ring of **4** is too polar to fit well into the hydrophobic deepest segment of the cavity, (2) relatively small differences between the potencies of their (*R*)- and (*S*)-enantiomers suggest the lack of H-bonding.

Antiparasitic Effects in *T. cruzi* Cells. *T. cruzi* is a unicellular eukaryotic parasite with the complex life cycle involving insect vectors and mammalian hosts. In insects, multiplying midgut epimastigotes transform into metacyclic trypomastigotes that infect humans. In humans, *T. cruzi* exists either as infective bloodstream trypomastigote or as multiplying intracellular amastigote (mostly in the heart muscles, but also in lungs, liver, spleen, and other organs and tissues). In this work the antiparasitic effects of the CYP51 inhibitors were analyzed in *T. cruzi* amastigotes within cardiomyocytes. Because compound **4** did not inhibit CYP51 activity *in vitro*, it was not selected for cellular experiments. For the majority of the other compounds, a very good correlation between their potencies to inhibit *T. cruzi* CYP51 enzyme in the reconstituted reaction *in vitro* and antiparasitic effects against the pathogen cells has been observed (Table 1, Figure 7), although quite pronounced activity of **5**, both the (*R*)- and (*S*)- enantiomers, might suggest that this structure can potentially have alternative target(s), better cellular permeability, or perhaps even an additional benznidazole-like mode of action (oxidative stress) due to the presence of the reactive nitro group.[28] Overall, strong antiparasitic activity combined with simple and cost-

effective syntheses make these compounds, particularly *T. cruzi* CYP51 inhibitors (*S*)-**2** (LFT) and (*R*)-**6** (LFD) as well as compound (*S*)-**5** (e.g., as an option for combination therapy) potentially promising new antichagasic drug candidates, which are worth testing in animal models.

■ **CONCLUSIONS**

By now *T. cruzi* sterol 14α-demethylase has been validated as essential for survival and multiplication of *T. cruzi*. The antifungal drugs posaconazole and ravuconazole may well pass clinical trials and reinforce the scarce arsenal of antichagasic chemotherapy. However, posaconazole is too expensive (>1,000 euro per patient), and ravuconazole still has unresolved problems with its bioavailability, which are most likely the major reason for its suppressive but not curative effect.[24] We hope that VNI, or one of its derivatives,[29] will also eventually proceed to translational research. Nevertheless, additional options for Chagas disease treatment are still highly needed, and therefore better understanding of the target CYP51 structure/function and inhibition should be greatly advantageous, particularly if the parasite acquires drug resistance upon treatment or if humans are infected with strains of *T. cruzi* that display natural drug resistance.[30]

This work, in addition to identifying new potential drug candidates, also provides the structural rationale for the compounds' inhibitory potencies and offers two alternative approaches that can be followed for further CYP51 structure-guided drug design and development. One approach is to use the high rigidity of the CYP51 substrate binding cavity. This feature is best displayed by the LFT/LFS costructures. Both these small molecules ensure their tight fit into the deepest segment of the CYP51 cavity via formation of the hydrogen bonding that not only strengthens the enzyme/inhibitor

Table 2. Data Collection and Refinement Statistics

T. cruzi CYP51−inhibitor complex	(*R*)-**6** (ligand PDB ID LFD)[a]	(*S*)-**2** (ligand PDB ID LFT)[b]	(*S*) **3** (ligand PDB ID LFS)[c]
	Data Collection		
Wavelength, Å	0.9787	0.9787	0.9787
Space group	P22(1)2(1)	P3(1)21	P3(1)21
Cell dimensions			
a, b, c, Å	59.900; 137.180; 152.430	62.953; 62.953; 222.435	62.582; 62.582; 221.068
α, β, γ, deg	90.00, 90.00, 90.00	90.00, 90.00, 120.00	90.00, 90.00, 120.00
No. of molec in asymm. unit	2	1	1
Solvent content, %	58.2	48.8	47.9
Resolution (last shell), Å	100−2.61 (2.67−2.61)	30−2.6 (2.69−2.6)	30−2.7 (2.8−2.7)
R_{merge} (last shell)	0.049 (0.558)	0.052 (0.675)	0.05 (0.583)
I/σ (last shell)	39.3 (2.9)	31.0 (3.0)	31.1 (3.4)
Completeness (last shell), %	99 (99)	99 (99)	99.5 (100)
Redundancy (last shell)	7.2 (5.6)	7.2 (7.3)	7.0 (7.2)
	Refinement		
Resolution, Å	30.0−2.62	30.0−2.74	28.8−2.7
R-factor	0.235	0.272	0.263
R-free	0.286	0.296	0.284
Reflections used	36336	13383	13738
Test set size, %	5.0	5.2	5.0
rms deviations from ideal geometry			
Bond lengths, Å	0.005	0.001	0.003
Bond angles, deg	1.14	0.93	1.28
Ramachandran plot			
Residues in favorable regions (%)	95.3	95.6	94.2
Residues in allowed regions (%)	99.8	100	100
Outliers (%)	0.2	0	0
	Model		
No. of atoms (mean *B*-factor, Å)	7377 (69.7)	3562 (90.5)	3541 (90.9)
Number of residues per molecule	A/B	A	A
Protein	449 (71.8)/450 (71.5)	434 (88.1)	434 (91.1)
Heme	1 (30.2)/(30.1)	1 (67.5)	1 (56.2)
Ligand	LFD 1 (75.9)/1 (81.9)	LFT 1 (57.8)	LFS 1 (72.7)
Water	24 (55.6)	25 (75.6)	4 (68.1)

[a]PDB code 4CK8. [b]PDB code 4CK9. [c]PDB code 4CKA.
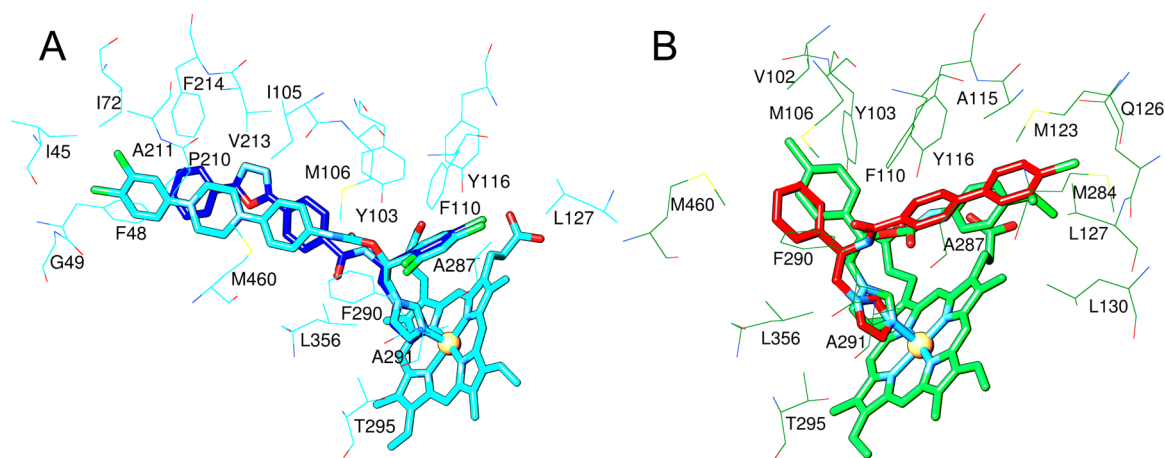
Figure 5. *T. cruzi* CYP51 active site illustrating interactions with LFD (cyan carbon atoms) and LFT (green carbon atoms). (A) Superimposition of CYP51 complexes with LFD and VNI (blue); (B) Superimposition of CYP51 complexes with LFT and VNF (red).

interaction but also disrupts the heme support from the protein moiety, thus affecting the environment (and most likely redox potential) of the catalytic iron. The second approach is to block the entrance into the CYP51 substrate access channel by building a surface binding subsite (as, e.g., in the *T. cruzi* complex with LFD or posaconazole[31]), since even weak van der Waals contacts between the enzyme and inhibitor in this area appear to prevent the substrate access channel from opening, the feature that must be functionally essential for sterol 14α-demethylase catalysis and therefore for the possibility of the substrate to replace the inhibitor in the enzyme active site.

Table 3. *T. cruzi* CYP51 Substrate Binding Cavity and Inhibitor-Contacting Residues

T. cruzi CYP51 active site		inhibitor-contacting residues (<4.5 Å)				
secondary structural elements	amino acid residues	posaconazole (3K10)[23]	(R)-6 [LFD] (4CK8)	(S)-2 [LFT] (4CK9)	(S)-3 [LFS] (4CKA)	VNF (3KSW)[23]
A′ helix (substrate access channel)	I45	I45	I45			
	V46	V46				
	F48	F48	F48			
	G49	G49	G49			
	K50					
	P52					
β1-1/β1-2 (substrate access channel)	I70					
	I72		*I72(4.8 Å)*			
	V77					
B′ helix (substrate binding cavity)	V102			*V102(4.7 Å)*		
	Y103	Y103	Y103	Y103	Y103	
	I105		I105			
	M106	M106	M106	M106	M106	M106
	F110	F110	F110	F110	F110	F110
B′/C loop (substrate binding cavity)	V114					
	A115			A115	A115	A115
	Y116	Y116	Y116	Y116	Y116	Y116
C helix (substrate binding cavity)				M123	M123	
	Q126			Q126	Q126	Q126
	L127	L127	L127	L127	L127	L127
	L130			L130	L130	L130
F″ helix (substrate access channel)	P210	P210	P210			
	A211	A211	A211			
	V213	V213	V213			
	F214	F214	F214			
I helix (substrate binding cavity)	M284			M284	M284	M284
	I285					
	V286					
	A287	A287	A287	A287	A287	A287
	F290	F290	F290	F290	F290	
	A291	A291	A291	A291	A291	A291
	H294					
	T295	T295	T295	T295	T295	T295
β4-1 (substrate binding cavity)	L356	L356	L356	L356	L356	L356
	L357	L357				
	M358	M358				
	V359					
	M360					
	R361					
β4 hairpin (substrate access channel)	Y457	Y457				
	H458	H458				
	T459	T459				
	M460	M460	M460	M460	M460	M460
	V461					V461
	V462					
Total no. of residues		25	19(20)	16 (17)	16	14

■ EXPERIMENTAL SECTION

Chemical Synthesis. All reagents and solvents were of high analytical grade and were purchased from Sigma-Aldrich (Milano, Italy). Melting points were determined on a Tottoli apparatus (Buchi) and are uncorrected. Infrared spectra were recorded on a Spectrum One ATR Perkin Elmer FT-IR spectrometer. ^{1}H and ^{13}C NMR spectra were acquired on a Bruker AVANCE-400 spectrometer at 9.4 T, in CDCl$_3$, CD$_3$OD, or DMSO-d_6, at 27 °C; chemical shift values are given in δ (ppm) relative to TMS as internal reference. Coupling constants are given in Hz. Mass analysis was carried out with a 2000 Q TRAP instrument (Applied Biosystems), a commercial hybrid triple-quadrupole linear ion-trap mass spectrometer (Q1q2QLIT), equipped with an ESI source and a syringe pump; the flow rate was 5 μL min^{-1}. The examined compounds were dissolved in methanol (10^{-5} M), and aqueous HCl was added just before the injection. The molecular peaks (m/z) have been observed as [M + H]$^+$. The stereochemistry of the (R)- and (S)-enantiomers as well as their enantiomeric excess (e.e.) was evaluated by chiral HPLC using a 250 mm × 4.6 mm i.d. Chiralcel OD column (Chiral Technologies Europe, Illkirch, France).[26] The HPLC apparatus consisted of a PerkinElmer (Norwalk, CT, USA) 200 LC pump equipped with a Rheodyne (Cotati, CA, USA) injector, a 20 mL sample loop, an HPLC Dionex CC-100 oven (Sunnyvale, CA, USA), and a Jasco (Jasco, Tokyo, Japan) model CD 2095 Plus UV/CD detector.
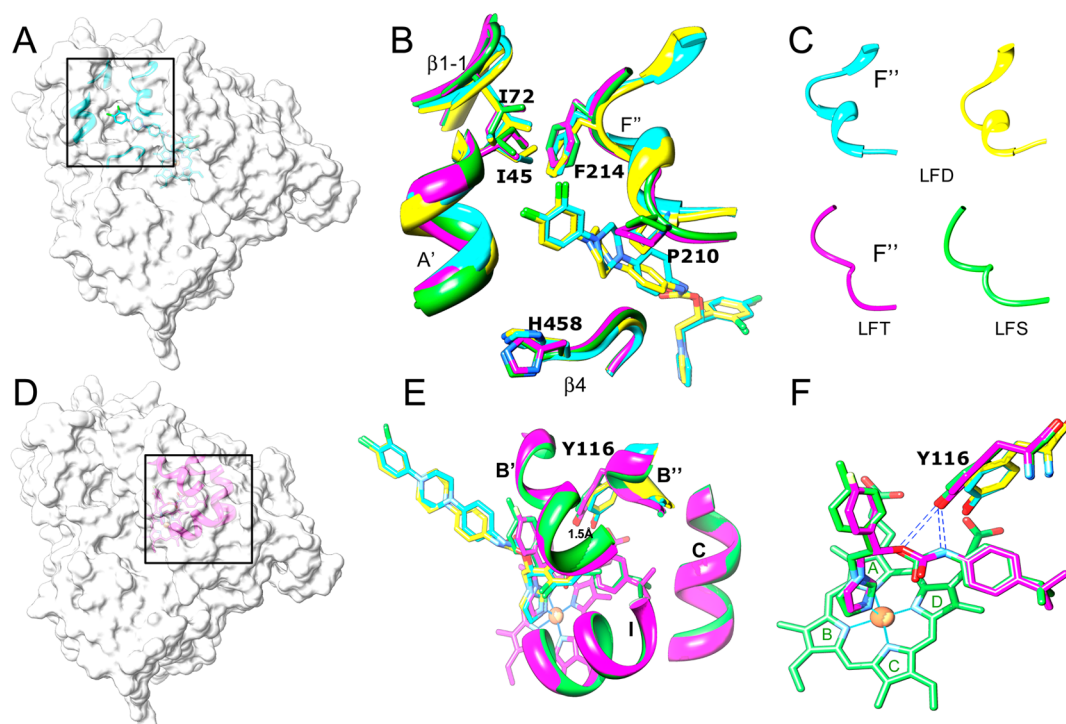
Figure 6. Two regions of the *T. cruzi* CYP51 molecule that strengthen the enzyme interaction with LFD (A−C) and LFT/LFS (D−F). Coloring: (yellow, cyan) complexes with LFD, molecules A and B, respectively; (green) complex with LFT; (pink) complex with LFS. (A,D) Semitransparent surface representation (P450 distal view). (B) Structural elements forming the substrate access channel entrance. (C) F″-helix. (E) Structural elements forming the deepest portion of the CYP51 binding cavity. (F) H-bonds between Y116 and the carbamic fragments of LFT and LFS.
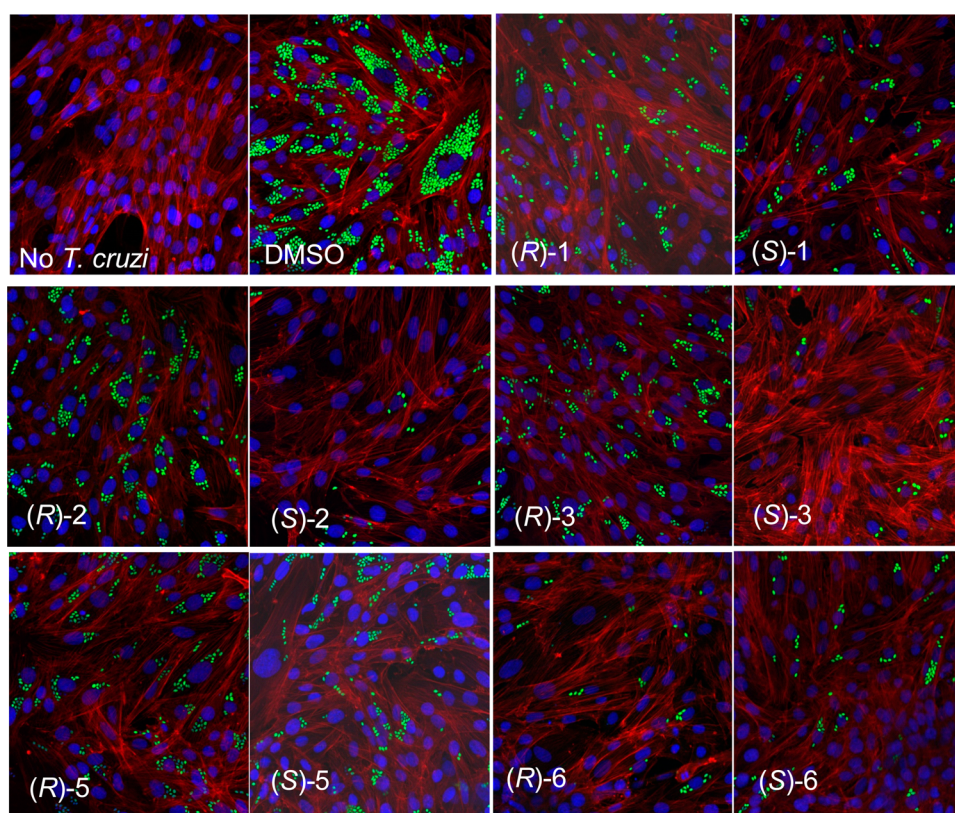

Figure 7. Fluorescence microscopic observation of *T. cruzi* multiplication inside cardiomyocytes treated with 4 nM of CYP51 inhibitors. Drugs were added to infected cardiomyocyte monolayers at 24 h of infection, and amastigote multiplication was observed at 72 h of infection. GFP-expressing *T. cruzi* amastigotes are green, cardiomyocyte nuclei are blue, and cardiomyocyte actin myofibrils are red.

Declaration of Purity. The purity of all the compounds, determined by combustion elemental analysis and reverse-phase HPLC, was >95%. Elemental analysis was performed using a PE 2400 (PerkinElmer) analyzer, and the analytical results were within ±0.4% of the theoretical values. The reverse-phase HPLC system was equipped with a dual-wavelength UV 2489 detector (Waters) set at 250 and 205 nm and a Symmetry C_{18} (3.5 μm) 4.6 mm × 75 mm column. The mobile phase was 55% 0.015 M potassium phosphate (pH 7.4) and 45% acetonitrile (v/v) with an isocratic flow rate of 1.0 mL/min.

Compound 2. The (R)- and (S)-enantiomers of 1-(4-chlorophenyl)-2-(1H-imidazol-1-yl)ethyl-4-isopropylphenylcarbamate were synthesized using the (R)- and (S)-enantiomers of 1-(4-chlorophenyl)-2-(1H-imidazol-1-yl)ethanol, respectively. One mmol of NaH was used to deprotonate 1 mmol of 1-(4-chlorophenyl)-2-(1H-imidazol-1-yl)ethanol suspended in 5 mL of anhydrous CH_3CN. The reaction mixture was stirred for 2 h at room temperature, and then 1.5 mmol of 4-isopropylphenyl isocyanate was added and stirred for 24 h at room temperature. The solvent was evaporated under reduced pressure, and the residue was washed with MeOH (3 × 3 mL). The mother liquor was dried and purified by silica gel column chromatography using CH_2Cl_2/MeOH (9:1) as eluent. The white solid was obtained with 45% yield (e.e. > 99%). Mp = 162−4 °C; IR 1722 cm^{-1}; ^{1}H NMR (DMSO-d_6): δ 9.75 (s, broad, 1H), 7.55 (s, 1H), 7.43 (d, 2H, J = 8.4 Hz), 7.36 (d, 2H, J = 8.4 Hz), 7.30 (d, 2H, J = 8.4 Hz), 7.15 (s, 1H), 7.12 (d, 2H, J = 8.4 Hz), 6.84 (s, 1H), 5.94 (m, 1H), 4.41 (m, 2H), 2.80 (m, 1H), 1.14 (d, 6H, J = 6.8 Hz); ^{13}C NMR (DMSO-d_6): δ 152.2, 144.3, 138.5, 135.3, 135.2, 134.2, 129.1, 127.4, 126.8, 126.4, 120.2, 119.1, 73.6, 52.4, 33.5, 24.0; Anal. Calcd for $C_{21}H_{22}ClN_3O_2$: C, 65.71; H, 5.78; N, 10.95. Found: (S)-form: C, 65.48; H, 5.78; N, 10.93; (R)-form: C, 65.80; H, 5.75; N, 10.91. MS-ESI$^+$ 384.8 [M + H]$^+$.

Compound 3. The (R)- and (S)-enantiomers of 1-(4-fluorophenyl)-2-(1H-imidazol-1-yl)ethyl-4-isopropylphenylcarbamate were prepared using the corresponding enantiomers of 1-(4-fluorophenyl)-2-(1H-imidazol-1-yl)ethanol following the procedure described for compound (R)-**2** and (S)-**2**. The white solid was obtained with 30% yield (e.e. > 99%). Mp = 200−202 °C; IR: 1715 cm^{-1}; ^{1}H NMR (DMSO-d_6): δ 9.74 (s, broad, 1H), 7.55 (s, 1H), 7.42 (m, 2H), 7.31 (d, 2H, J = 8.5 Hz), 7.22 (m, 2H), 7.15 (s, 1H), 7.13 (d, 2H, J = 8.5 Hz), 6.84 (s, 1H), 5.94 (t, 1H, J = 5.4 Hz), 4.43 (m, 2H), 2.80 (m, 1H), 1.16 (d, 6H, J = 6.9 Hz); ^{13}C NMR (CD$_3$OD): δ 162.7 (J = 245 Hz), 153.0, 143.8, 137.8, 136.0, 133.5 (J = 3 Hz), 128.0 (J = 9 Hz), 127.5, 126.3, 120.2, 118.8, 115.1 (J = 21 Hz), 74.2, 51.3, 33.4, 23.1; Anal. Calcd for $C_{21}H_{22}FN_3O_2$: C, 68.65; H, 6.04; N, 11.44. Found: (S)-form: C, 68.39; H, 6.05; N, 11.42; (R)-form: C, 68.61; H, 6.15; N, 11.63. MS-ESI$^+$ 368.4 [M + H]$^+$.

Compound 4. The (R)- and (S)-enantiomers of 1-(4-fluorophenyl)-2-(1H-imidazol-1-yl)ethanol were also used for synthesis of (R)- and (S)-1-(4-fluorophenyl)-2-(1H-imidazol-1-yl)ethyl 3-(1H-imidazol-1-yl)propylcarbamate. 0.5 mmol of 1-(4-fluorophenyl)-2-(1H-imidazol-1-yl)ethanol was suspended in 5 mL of anhydrous CH_3CN, and then 0.25 mmol of triphosgene was added and the solution was stirred overnight at room temperature. The reaction mixture was treated with Et_2O, producing a white precipitate of 1-(4-fluorophenyl)-2-(1H-imidazol-1-yl)ethyl chloroformate. The solvent was removed by decantation; the precipitate was washed with Et_2O (2 × 5 mL) and dissolved in anhydrous CH_3CN. Then, 1.6 mmol of TEA and 0.8 mmol of 3-(1H-imidazol-1-yl)propan-1-amine were added to the solution. The reaction was stirred overnight at room temperature. The crude mixture was diluted with H_2O (5 mL), and the aqueous layer was extracted with $CHCl_3$ (3 × 10 mL). The combined organic layers were dried under anhydrous sodium sulfate, and the solvent was evaporated under reduced pressure. The crude product was purified by silica gel column chromatography using CH_2Cl_2/MeOH (8:2). The white solid was obtained with the yield 80% (e.e. > 98%). Mp = 101−103 °C; IR: 1710 cm^{-1}; ^{1}H NMR (CD$_3$OD): δ 7.61 (s, 1H), 7.56 (s, 1H), 7.36 (m, 2H), 7.11 (m, 4H), 6.96 (s, 1H), 6.94 (s, 1H), 5.92 (m, 1H), 4.40 (m, 2H), 4.00 (t, 2H, J = 6.8 Hz), 3.05 (m, 2H), 1.93 (m, 2H, J = 6.8 Hz); ^{13}C NMR (CDCl$_3$): δ 162.8 (J = 247 Hz), 155.2,

137.9, 137.2, 133.0 (J = 2 Hz), 129.3, 128.9, 128.0 (J = 8 Hz), 119.8, 118.8, 115.8 (J = 22 Hz), 74.05, 51.9, 44.4, 38.2, 31.2. Anal. Calcd for $C_{18}H_{20}FN_5O_2$: C, 60.49; H, 5.64; N, 19.60. Found: (S)-form: C, 60.49; H, 5.65; N, 19.61; (R)-form: C, 60.60; H, 5.59; N, 19.63. MS-ESI$^+$ 358.13 [M + H]$^+$.

Compound 5. The (R)- and (S)-enantiomers of 1-(4-chlorophenyl)-(1H-imidazol-1-yl)ethyl 4-(4-nitrophenylthio)phenylcarbamate were prepared by suspending 1 mmol of (R)- or (S)-1-(4-chlorophenyl)-2-(1H-imidazol-1-yl)ethanol, respectively, in 5 mL of anhydrous CH_3CN. Then 0.5 mmol of triphosgene was added and the solution was treated as described above except that 3 mmol of TEA and 0.8 mmol of 4-((4-nitrophenyl)thio)aniline were added to 1-(4-chlorophenyl)-2-(1H-imidazol-1-yl)ethyl chloroformate. The crude product was purified by silica gel column chromatography using $CHCl_3$/MeOH (9:1). The yellow solid was obtained with the yield 85% (e.e. > 98%). Mp = 100−102 °C; IR: 1727 cm^{-1}; ^{1}H NMR (CD$_3$OD): δ 8.07 (d, 2H, J = 9.05 Hz), 7.57 (m, 3H), 7.49 (d, 2H, J = 8.8 Hz), 7.38 (m, 4H), 7.18 (m, 3H), 6.96 (s, 1H), 6.04 (t, 1H, J = 6.2 Hz), 4.49 (m, 2H); ^{13}C NMR (DMSO-d_6): δ 152.6, 149.2, 145.3, 141.1, 138.4, 137.1, 136.5, 133.4, 128.9, 128.7, 128.6, 126.4, 124.7, 122.2, 120.5, 120.1, 74.6, 50.7. Anal. Calcd for $C_{24}H_{19}ClN_4O_4S$: C, 58.24; H, 3.87; N, 11.32. Found: (S)-form: C, 58.34; H, 3.88; N, 11.33; (R)-form: C: 58.01; H, 3.99; N, 11.30. MS-ESI$^+$ 495.07 [M + H]$^+$.

Compound 6. The (R)- and (S)-enantiomers of 1-(2,4-dichlorophenyl)-2-(1H-imidazol-1-yl)ethyl 4-[4-(3,4-dichlorophenyl)-piperazin-1-yl]phenylcarbamate were prepared using 1 mmol of (R)- or (S)-1-(2,4-dichlorophenyl)-2-(1H-imidazol-1-yl)ethanol to obtain 1-(2,4-dichlorophenyl)-2-(1H-imidazol-1-yl)ethyl chloroformate following the procedure described for compound **5**. The synthesis of 4-[4-(3,4-dichlorophenyl)piperazin-1-yl] anilinium chloride was carried out by condensation of 1 mmol of 1-(3,4-dichlorophenyl)-piperazine dissolved in 5 mL of CH_3CN and 2.5 mmol of 1-fluoro-4-nitrobenzene (see Scheme 2). After refluxing for 2 h, the solvent was removed and the crude residue was purified by silica gel column chromatography, using CH_2Cl_2/MeOH (9:1) as eluent. 1-(3,4-Dichlorophenyl)-4-(4-nitrophenyl)piperazine was obtained with 80% yield. Then 1-(3,4-dichlorophenyl)-4-(4-nitrophenyl)piperazine was suspended in 90 mL of MeOH and reduced to amine by hydrogenation in the presence of 10% Pd/C as catalyst at room temperature, 50 psi for 4 h. The catalyst was removed by filtration, and the solution was bubbled with gaseous HCl for 1 h at 0 °C. The solvent was evaporated under reduced pressure to give 4-[4-(3,4-dichlorophenyl)piperazin-1-yl] anilinium chloride with 90% yield. 0.8 mmol of 4-[4-(3,4-dichlorophenyl)piperazin-1-yl] anilinium chloride and 3 mmol of TEA was added to the (R)- or (S)-1-(2,4-dichlorophenyl)-2-(1H-imidazol-1-yl)ethyl chloroformate dissolved in 5 mL of anhydrous CH_3CN. The reaction was stirred overnight at room temperature, the crude mixture diluted with H_2O, and the aqueous layer extracted with CH_2Cl_2 (3 × 10 mL). The combined organic layers were dried under anhydrous sodium sulfate, and the solvent was evaporated. The crude product was purified by silica gel column chromatography using CH_2Cl_2/MeOH (9.5:0.5) as eluent. The white solid was obtained with 70% yield (e.e. > 98%). Mp = 220−225 °C; IR: 1720 cm^{-1}; ^{1}H NMR (DMSO-d_6): δ 9.75 (s broad, 1H), 7.69 (d, 1H, J = 2.0 Hz), 7.54 (s, 1H), 7.44−7.39 (m, 2H), 7.29−7.18 (m, 4H), 7.11 (s, 1H), 6.98 (dd, 1H, J = 8.9 Hz, J = 2.8 Hz), 6.93 (d, 2H, J = 8.4 Hz), 6.86 (s, 1H), 6.11 (m, 1H), 4.46 (m, 2H), 3.38 (m, 4H), 3.36 (m, 4H); ^{13}C NMR (CD$_3$OD): δ 150.5, 148.7, 138.8, 135.1, 133.0, 132.9, 132.0, 130.5, 129.6, 129.2, 128.1, 127.9, 125.5, 122.5, 120.4, 120.3, 117.5, 117.2, 116.3, 115.5, 70.9, 50.6, 49.8, 48.9; Anal. Calcd for $C_{28}H_{25}Cl_4N_5O_2$: C, 55.56; H, 4.16; N, 11.57. Found: (S)-form: C, 55.65; H, 4.16; N, 11.56; (R)-form: 55.68; H, 4.15; N, 11.69. MS-ESI$^+$ 605.98 [M + H]$^+$.

CYP51 Expression and Purification. For functional studies, including ligand binding and enzymatic activity assays, we used the full-length Tulahuen T. cruzi CYP51 (GenBank IDs AY856083) expression construct, designed and purified as previously described in ref 21. For crystallization purposes, we utilized the T. cruzi CYP51 N-terminal truncated construct where the membrane anchor sequence

(first 31 residues upstream of P32) was replaced with the 5-amino acid sequence fragment MAKKT-.[23] In all cases the CYP51 gene was His-tag-engineered at the C-terminus, subcloned into the pCW expression vector, and expressed in the *E. coli* strain HMS174(DE3) (Novagen).

CYP51 Spectral Ligand Binding Assay. Changes in the *T. cruzi* CYP51 Soret band absorbance spectra upon titration with each compound were recorded at 25 °C using a dual beam Shimadzu UV-240IPC spectrophotometer. The P450 concentration was determined from the Soret band intensity of the reduced CO complexes using visible absorption difference spectroscopy, $\Delta\varepsilon 450-490 = 91$ mM^{-1} cm^{-1}.[32] Spectral titrations were performed at ~1 μM P450 concentration in a 20 mM K-phosphate buffer, pH 7.4, containing 200 mM NaCl and 0.1 mM EDTA. The optical path length was 5 cm. Ligand binding was monitored as a red shift in the Soret band maximum reflecting coordination of the heterocyclic nitrogen to the P450 heme iron.[17] Difference spectra were generated by recording the P450 absorbance in a sample cuvette versus the absorbance in a reference cuvette, both containing the same amount of the protein. Compounds were added to the sample cuvette in the concentration range 0.2−2.0 μM from 0.4 mM stock solutions in DMSO. The titration step was 0.2 μM. At each step, the corresponding volume of DMSO was added to the reference cuvette. The apparent dissociation constants of the enzyme−inhibitor complexes (spectral dissociation constants (K_s)) and the magnitude of spectral binding (binding efficiency ($\Delta A_{max}/K_s$)) were calculated with GraphPad Prism (Graph-Pad Software, La Jolla, CA) using a quadratic function for tight binding ligands by fitting the data for the ligand-induced spectral change (peak to trough absorbance changes in the difference spectra (ΔA)) versus total ligand concentration to the following equation:

$$\Delta A = (\Delta A_{max}/2E)((L + E + K_s) \\ - ((L + E + K_s)^2 - 4LE)^{0.5})$$

where [L] and [E] are the concentrations of the ligand and the enzyme used for the titration, respectively.[20]

CYP51 Activity Assay. The enzymatic activity of *T. cruzi* CYP51 was reconstituted *in vitro* as described previously using eburicol (24-methylenedihydrolanosterol) as the substrate.[21] Briefly, the reaction mixture contained 1 μM CYP51, 2 μM cytochrome P450 reductase (CPR), 100 μM dilauroyl-α-phosphatidylcholine, 0.4 mg/mL iso-cytrate dehydrogenase, and 25 mM sodium isocitrate in 20 mM MOPS (pH 7.4), 50 mM KCl, 5 mM MgCl$_2$, and 10% glycerol. After addition of the [^{3}H]-radiolabeled sterol substrate (~2,000 cpm/nmol, final concentration 50 μM), the mixture was preincubated for 5 min at 37 °C; the reaction was initiated by addition of 100 μM NADPH and stopped by extraction of the sterols with ethyl acetate. The reaction products were analyzed by a reverse-phase HPLC system (Waters) equipped with a β-RAM detector (INUS Systems, Inc.) using a Nova Pak C18 column. The potencies of the compounds to inhibit *T. cruzi* CYP51 activity were compared as inhibition of the substrate conversion in a 1 h reaction at molar ratio enzyme/substrate/inhibitor = 1:50:2, as these conditions were shown previously to allow distinguishing the most potent compounds.[17,20,23]

T. cruzi Cellular Growth Inhibition Assay. A cellular *T. cruzi* infection assay was performed using highly invasive 20A clone of the Tulahuen strain of *T. cruzi*, which was shown to infect >98% of exposed cardiomyocytes.[33] *T. cruzi* trypomastigotes expressing green fluorescent protein (GFP) were generated as described.[23] Trypomas-tigotes were used to infect cardiomyocyte monolayers in 96-well tissue culture plates and in 8-well LabTech tissue culture chambers in triplicate at the ratio of 10 parasites per cell as described.[24,34] Cultures were incubated with DMEM supplemented with 10% fetal bovine serum (FBS) as described.[24] Unbound trypomastigotes were removed by washing the cellular monolayers with DMEM; and infected monolayers were exposed to several concentrations of the inhibitors (from 1 nM to 25 nM), dissolved in DMSO/DMEM free of phenol red in triplicate at 24 h of infection, and cocultured in DMEM + 10% FBS for 48 h to observe parasite multiplication. Posaconazole was used as a control. At 72 h of infection, the cardiomyocyte monolayers were washed with phosphate-buffered saline, and the infection was

fluorimetically quantified as Relative Fluorescence Units (RFU) using a Synergy HT fluorometer (Biotek Instruments).[23,34] For fluorescence microscopy observation, the infection assays were performed in 8-well LabTech tissue culture chambers in triplicate; after 72 h of infection the cardiomyocyte monolayers were fixed with 2.5% paraformaldehyde and stained with 4′,6-diamidino-2-phenyl-indole, to visualize DNA, and with Alexa fluor 546 phalloidin (Invitrogen) to visualize cardiomyocyte actin myofibrils as described.[24]

X-ray Crystallography. The initial screening of crystallization conditions was performed using Hampton Research crystallization kits. Twenty mM stock solutions of compounds (*S*)-**2**, (*S*)-**3**, and (*R*)-**6** in DMSO were added at 2-fold molar excess to the 350 μM solution of *T. cruzi* CYP51 in 20 mM K-phosphate buffer, pH 7.2, containing 200 mM NaCl, 0.1 mM EDTA, 10% glycerol, and 0.048 mM *n*-tridecyl-β-d-maltoside. Crystals were grown at 23 °C using the hanging-drop vapor diffusion method, cryoprotected by plunging them into a drop of reservoir solution supplemented with 20% glycerol, flash-frozen in liquid nitrogen, and then prescreened on a Bruker Microstar microfocus rotating-anode X-ray generator/Proteum PT135 CCD area detector. Crystals that diffracted to ~3.0 Å resolution were subsequently used for the data collection at the synchrotron (Advanced Photon Source, Argonne National Laboratory, IL) on beamline 21ID-F at 100 K. The diffraction images were integrated using Mosflm and scaled with Aimless (CCP4 Program Suite 6.3.0[35]) in the P22(1)2(1) space group in the case of LFD (to resolution of 2.61 Å) and in the P3(1)21 space group in the cases of LFT (2.60 Å) and LFS (2.70 Å). Solvent content was estimated with a Matthews probability calculator. The crystal structures were determined by molecular replacement in PhaserMR using the atomic coordinates of the posaconazole-bound *T. cruzi* CYP51 structure (PDB code 3K1O) as the search model. In each case Phaser found a single solution, with one protein molecule in the asymmetric unit in the cocrystals of *T. cruzi* CYP51 with (*S*)-**2** and (*S*)-**3** and with two protein molecules in the asymmetric unit in the cocrystals of *T. cruzi* CYP51 with (*R*)-**6**. The models were built and refined with COOT and REFMAC5, respectively, from the CCP4 Program Suite 6.3.0.[35] Data collection and refinement statistics are shown in Table 2. The electron densities for each inhibitor were well-defined in all cases, showing full occupancy and opposite orientation of short (*S*)-**2**/(*S*)-**3** versus long (*R*)-**6** (the $2F_o - F_c$ electron density maps for (*R*)-**6** and (*S*)-**3** weighted at 1.5σ are shown in the graphical abstract).

■ ASSOCIATED CONTENT

ⓢ Supporting Information
Two figures showing (1) surface binding subsites formed in the complexes of *T. cruzi* CYP51 with LFD and with posaconazole and (2) the influence of binding of LFD and LFT on *T. cruzi* CYP51 flexibility. This material is available free of charge via the Internet at http://pubs.acs.org.

Accession Codes
The coordinates and structure factors of *T. cruzi* CYP51 in complex with compounds (*R*)-**6** (ligand PDB ID LFD), (*S*)-**2** (LFT), and (*S*)-**3** (LFS) have been deposited in the Protein Data Bank, PDB codes 4CK8, 4CK9, and 4CKA, respectively (http://www.rcsb.org).

■ AUTHOR INFORMATION

Corresponding Author
*Vanderbilt University, 622 RRB, 23rd@Pierce, Nashville, TN, 37232, USA. Tel: 615-343-1373, e-mail: galina.i.lepesheva@vanderbilt.edu.

Present Address
#(L.F.) Department of "Chimica e Tecnologie del Farmaco", Sapienza University of Rome, Rome 00185, Italy.

Notes
The authors declare no competing financial interest.

■ ABBREVIATIONS USED

CYP, cytochrome P450; CYP51, sterol 14α-demethylase; *T. cruzi*, *Trypanosoma cruzi*; EC$_{50}$, drug concentration that gives half-maximal response in cellular growth reduction; GFP, green fluorescent protein; RuCl(*p*-cymene)[(*S,S*)-Ts-DPEN], (*S,S*)-*N*-(*p*-toluenesulfonyl)-1,2-diphenylethanediamine(chloro)(*p*-cymene)ruthenium(II); VNI, ((*R*)-*N*-(1-(2,4-dichlorophenyl)-2-(1*H*-imidazol-1-yl)ethyl)-4-(5-phenyl-1,3,4-oxadiazol-2-yl)-benzamide); VNF, ((*R*)-*N*-(2-(1*H*-imidazol-1-yl)-1-phenyleth-yl)-4′-chlorobiphenyl-4-carboxamide)

■ REFERENCES

(1) Lepesheva, G. I. Design or screening of drugs for the treatment of Chagas disease: what shows the most promise? *Expert Opin. Drug Discovery* **2013**, *8*, 1479−1489.

(2) WHO. http://www.who.int/neglected_diseases/9789241564540/en/, 2013, last accessed May 7, 2014.

(3) Clayton, J. Chagas disease: pushing through the pipeline. *Nature* **2010**, *465*, S12−S15.

(4) Leslie, M. Drug developers finally take aim at a neglected disease. *Science* **2011**, *333*, 933−935.

(5) Klein, N.; Hurwitz, I.; Durvasula, R. Globalization of Chagas disease: a growing concern in nonendemic countries. *Epidemiol. Res. Int.* **2012**, 1−13.

(6) Bern, C.; Kjos, S.; Yabsley, M. J.; Montgomery, S. P. *Trypanosoma cruzi* and Chagas' disease in the United States. *Clin. Microbiol. Rev.* **2011**, *24*, 655−681.

(7) Hotez, P. J. Neglected infections of poverty in the United States of America. *PLoS Neglected Trop. Dis.* **2008**, *2*, e256.

(8) Barry, M. A.; Bezek, S.; Serpa, J. A.; Hotez, P. J.; Woc-Colburn, L. Neglected infections of poverty in Texas and the rest of the United States: management and treatment options. *Clin. Pharmacol. Ther.* **2012**, *92*, 170−181.

(9) Filardi, L. S.; Brener, Z. Susceptibility and natural resistance of *Trypanosoma cruzi* strains to drugs used clinically in Chagas disease. *Trans. R. Soc. Trop. Med. Hyg.* **1987**, *81*, 755−759.

(10) Rassi, A., Jr.; Rassi, A.; Marin-Neto, J. A. Chagas disease. *Lancet* **2012**, *375*, 1388−1402.

(11) Bern, C. Antitrypanosomal therapy for chronic Chagas' disease. *N. Engl. J. Med.* **2011**, *364*, 2527−2534.

(12) Lepesheva, G. I.; Waterman, M. R. Sterol 14 alpha-demethylase cytochrome P450 (CYP51), a P450 in all biological kingdoms. *Biochim. Biophys. Acta* **2007**, *1770*, 467−477.

(13) Urbina, J. A. Ergosterol biosynthesis and drug development for Chagas disease. *Mem. Inst. Oswaldo Cruz* **2009**, *104* (Suppl 1), 311−318.

(14) Hucke, O.; Gelb, M. H.; Verlinde, C. L. M. J.; Buckner, F. S. The Protein farnesyltransferase inhibitor tipifarnib as a new lead for the development of drugs against Chagas disease. *J. Med. Chem.* **2005**, *48*, 5415−5418.

(15) Buckner, F.; Bahia, M. T.; Suryadevara, P. K.; White, K. L.; Shackleford, D. M.; Chennamaneni, N. K.; Hulverson, M. A.; Laydbak, J. U.; Chatelain, E.; Scandale, I.; Verlinde, C. L.; Charman, S. A.; Lepesheva, G. I.; Gelb, M. H. Pharmacological characterization, structural studies, and *in vivo* activity of anti-Chagas disease lead compounds derived from tipifarnib. *Antimicrob. Agents Chemother.* **2012**, *56*, 4914−4921.

(16) Buckner, F.; Yokoyama, K.; Lockman, J.; Aikenhead, K.; Ohkanda, J.; Sadilek, M.; Sebti, S.; Van Voorhis, W.; Hamilton, A.; Gelb, M. H. A class of sterol 14-demethylase inhibitors as anti-*Trypanosoma cruzi* agents. *Proc. Natl. Acad. Sci. U. S. A.* **2003**, *100*, 15149−15153.

(17) Lepesheva, G. I.; Ott, R. D.; Hargrove, T. Y.; Kleshchenko, Y. Y.; Schuster, I.; Nes, W. D.; Hill, G. C.; Villalta, F.; Waterman, M. R. Sterol 14 alpha-demethylase as a potential target for antitrypanosomal therapy: Enzyme inhibition and parasite cell growth. *Chem. Biol.* **2007**, *14*, 1283−1293.

(18) Andriani, G.; Amata, E.; Beatty, J.; Clements, Z.; Coffey, B. J.; Courtemanche, G.; Devine, W.; Erath, J.; Juda, C. E.; Wawrzak, Z.; Wood, J. T.; Lepesheva, G. I.; Rodriguez, A.; Pollastri, M. P. Antitrypanosomal lead discovery: identification of a ligand-efficient inhibitor of *Trypanosoma cruzi* CYP51 and parasite growth. *J. Med. Chem.* **2013**, *56*, 2556−2567.

(19) Konkle, M. E.; Hargrove, T. Y.; Kleshchenko, Y. Y.; von Kries, J. P.; Ridenour, W.; Uddin, M. J.; Caprioli, R. M.; Marnett, L. J.; Nes, W. D.; Villalta, F.; Waterman, M. R.; Lepesheva, G. I. Indomethacin amides as a novel molecular scaffold for targeting *Trypanosoma cruzi* sterol 14α-demethylase. *J. Med. Chem.* **2009**, *52*, 2846−2853.

(20) Hargrove, T. Y.; Wawrzak, Z.; Alexander, P. W.; Chaplin, J. H.; Keenan, M.; Charman, S. A.; Waterman, M. R.; Chatelain, E.; Lepesheva, G. I. Complexes of *Trypanosoma cruzi* sterol 14α-demethylase (CYP51) with two pyridine-based drug candidates for Chagas disease: Structural basis for pathogen selectivity. *J. Biol. Chem.* **2013**, *288*, 31602−31615.

(21) Lepesheva, G. I.; Zaitseva, N. G.; Nes, W. D.; Zhou, W.; Arase, M.; Liu, J.; Hill, G. C.; Waterman, M. R. CYP51 from *Trypanosoma cruzi*: a phyla-specific residue in the B′ helix defines substrate preferences of sterol 14alpha-demethylase. *J. Biol. Chem.* **2006**, *281*, 3577−85.

(22) Lepesheva, G. I.; Park, H. W.; Hargrove, T. Y.; Vanhollebeke, B.; Wawrzak, Z.; Harp, J. M.; Sundaramoorthy, M.; Nes, W. D.; Pays, E.; Chaudhuri, M.; Villalta, F.; Waterman, M. R. Crystal structures of *Trypanosoma brucei* sterol 14 alpha-demethylase and implications for selective treatment of human infections. *J. Biol. Chem.* **2010**, *285*, 1773−1780.

(23) Lepesheva, G. I.; Hargrove, T. Y.; Anderson, S.; Kleshchenko, Y.; Furtak, V.; Wawrzak, Z.; Villalta, F.; Waterman, M. R. Structural insights into inhibition of sterol 14alpha-demethylase in the human pathogen *Trypanosoma cruzi*. *J. Biol. Chem.* **2010**, *285*, 25582−25590.

(24) Villalta, F.; Dobish, M. C.; Nde, P. N.; Kleshchenko, Y. Y.; Hargrove, T. Y.; Johnson, C. A.; Waterman, M. R.; Johnston, J. N.; Lepesheva, G. I. VNI cures acute and chronic experimental Chagas disease. *J. Infect. Dis.* **2013**, *208*, 504−511.

(25) De Vita, D.; Scipione, L.; Tortorella, S.; Mellini, P.; Di Rienzo, B.; Simonetti, G.; D'Auria, F. D.; Panella, S.; Cirilli, R.; Di Santo, R.; Palamara, A. T. Synthesis and antifungal activity of a new series of 2-(1*H*-imidazol-1-yl)-1-phenylethanol derivatives. *Eur. J. Med. Chem.* **2012**, *49*, 334−342.

(26) Friggeri, L.; Scipione, L.; Costi, R.; Kaiser, M.; Moraca, F.; Zamperini, C.; Botta, B.; Di Santo, R.; De Vita, D.; Brun, R.; Tortorella, S. New promising compounds with *in vitro* nanomolar activity against *Trypanosoma cruzi*. *ACS Med. Chem. Lett.* **2013**, *4*, 538−541.

(27) Lepesheva, G. I.; Waterman, M. R. Structural basis for conservation in the CYP51 family. *Biochim. Biophys. Acta* **2011**, *1814*, 88−93.

(28) Álvarez, G.; Varela, J.; Márquez, P.; Gabay, M.; Arias Rivas, C. E.; Cuchilla, K.; Echeverría, G. A.; Piro, O. E.; Chorilli, M.; Leal, S. M.; Escobar, P.; Serna, E.; Torres, S.; Yaluff, G.; Vera de Bilbao, N. I.;

González, M.; Cerecetto, H. Optimization of antitrypanosomatid agents: identification of nonmutagenic drug candidates with *in vivo* activity. *J. Med. Chem.* **2014**, *57*, 3984−3999.

(29) Hargrove, T. Y.; Kim, K.; de Nazaré Correia Soeiro, M.; da Silva, C. F.; Batista, D. G.; Batista, M. M.; Yazlovitskaya, E. M.; Waterman, M. R.; Sulikowski, G. A.; Lepesheva, G. I. CYP51 structures and structure-based development of novel, pathogen-specific inhibitory scaffolds. *Int. J. Parasitol Drugs Drug Resist.* **2012**, *2*, 178−186.

(30) Soeiro, M. d. N.; de Souza, E. M.; da Silva, C. F.; Batista, D. d. G. J.; Batista, M. M.; Pavão, B. P.; Araújo, J. S.; Lionel, J.; Britto, C.; Kim, K.; Sulikowski, G.; Hargrove, T. Y.; Waterman, M. R; Lepesheva, G. I. *In vitro* and *in vivo* studies of the antiparasitic activity of sterol 14α-demethylase (CYP51) inhibitor VNI against drug-resistant strains of *Trypanosoma cruzi. Antimicrob. Agents Chemother.* **2013**, *57*, 4151−4163.

(31) Lepesheva, G. I.; Villalta, F.; Waterman, M. R. Targeting *Trypanosoma cruzi* sterol 14α-demethylase (CYP51). *Adv. Parasitol.* **2011**, *75*, 65−87.

(32) Omura, T.; Sato, R. The carbon monoxide-binding pigment of liver microsomes. I. Evidence for Its hemoprotein nature. *J. Biol. Chem.* **1964**, *239*, 2370−2378.

(33) Lima, M. F.; Villalta, F. *Trypanosoma cruzi* trypomastigote clones differentially express a parasite cell adhesion molecule. *Mol. Biochem. Parasitol.* **1989**, *33*, 159−170.

(34) Johnson, C. A.; Rachakonda, G.; Kleshchenko, Y. Y.; Nde, P. N.; Madison, M. N.; Pratap, S.; Cardenas, T. C.; Taylor, C.; Lima, M. F.; Villalta, F. Cellular response to *Trypanosoma cruzi* infection induces secretion of defensin α-1, which damages the flagellum, neutralizes trypanosome motility, and inhibits infection. *Infect. Immun.* **2013**, *81*, 4139−4148.

(35) Collaborative Computational Project, N. The CCP4 suite: programs for protein crystallography. *Acta Crystallogr., D: Biol. Crystallogr.* **1994**, *50*, 760−763.